CALCIFICATION AT THE INTERFACE BETWEEN TITANIUM IMPLANTS AND BONE: OBSERVATION WITH CONFOCAL LASER SCANNING MICROSCOPY

Tetsunari Nishikawa, DDS, PhD
Kazuya Masuno, DDS, MS
Masahiko Mori, DDS, PhD
Yasuhiro Tajime, DDS
Kenji Kakudo, DDS, PhD
Akio Tanaka, DDS, PhD

KEY WORDS

Titanium implants
Bone calcification
Histomorphometry

It has not been previously possible to observe bone formation in undecalcified sections with titanium implants at high magnification because of the difficulty in sectioning bone together with implants. A method for examining the bone-implant interface in undecalcified sections is described in which implants are left in situ and confocal laser scanning microscopy (CLSM) is used to examine both the implant surface and adjacent bone. Pulsing of animals at different times with the fluorescent dyes calcein and alizarin red permitted assessment of temporal patterns of bone formation by CLSM. Reflectivity of the polished implant surface permitted accurate assessment of the position of the implant relative to labeled bone. The analysis showed that bone first formed as thin processes towards and across the implant surface, followed by further bone formation behind these processes. The interface between calcified bone tissue and the implant surface was characterized by a 10-μm space. The CLSM technique enabled detailed observations of new bone formation at the titanium implant interface.

Tetsunari Nishikawa, DDS, PhD, *is an associate professor and* ***Kazuya Masuno, DDS, MS,*** *is a researcher at the Department of Oral Pathology,* ***Masahiko Mori, DDS, PhD,*** *is a visiting professor,* ***Yasuhiro Tajime, DDS,*** *is a PhD student,* ***Kenji Kakudo, DDS, PhD,*** *is a professor at the Second Department of Oral and Maxillofacial Surgery, and* ***Akio Tanaka, DDS, PhD,*** *is a professor at the Department of Oral Pathology, Osaka Dental University, 8-1 Kuzuhahanazono-cho, Hirakata-shi, Osaka, 573-1121, Japan. Address correspondence to Dr Nishikawa (e-mail: tetsu-n@cc.osaka-dent.ac.jp).*

INTRODUCTION

Many studies have noted the high biocompatibility of titanium dental implants.[1,2] Several methods of modifying machined implant surfaces have been reported to improve bone formation, including coating with hydroxyapatite,[3] $CaTiO_2$,[4] acid treatment,[5] and mechanical roughening.[6] Continuing research in osseointegration has increased the need for improved morphological observations of the bone-titanium interface.[7]

Osseointegration is variously reported to represent direct contact between bone and implant[8] or alternatively to involve interposition of a small amount of soft tissue between the implant and

bone from 95 to 200 nm in width.[9,10] Such observations have been made using thin sections by light microscopy,[5,9] radiography,[11] or scanning electron microscopy.[4]

Because titanium implants cannot be dissolved with acid or chelate, it is technically difficult to prepare thin sections. Consequently, a range of methods has been previously used to remove implants before the preparation of thin sections.[8,11–13] Recently, however, methods for the preparation of thin sections with a diamond saw and polishing have been developed that permit implants to be left in situ during sectioning.[6,9,14,15] Nonetheless, fine observations are limited by these methods because of the extreme fragility of these undecalcified specimens.[16]

Separately, confocal laser scanning microscopy (CLSM) has been used to study undecalcified specimens of bone labeled during deposition with calcein or alizarin red, thus allowing the calcification of new bone to be morphologically characterized in relatively thick sections of around 500 μm.[17] In addition, bone formation around implants has been described,[16,18] and tetracycline labeling has been used to detect bone formation in apparent contact with the implant surface.[19] However, it must be difficult to observe the simultaneous image of both implant and bone formation at high magnification.

In the present study, bone defects were created in the maxillae of beagle dogs, and implants were placed together with autologous bone fragments containing platelet-rich plasma (PRP) to promote bone formation.[20] Alizarin red and calcein were administered to facilitate observation by CLSM of new bone formation. The goal of this study was to determine whether bone formation could be observed at a high level of microscopic resolution without interrupting the bone-implant interface.

MATERIALS AND METHODS

Experimental animals

This study was recognized by the Animal Research Committee of Osaka Dental University and was conducted in accordance with the Guidelines for Animal Research at Osaka Dental University. Three female beagle dogs weighing 10 to 12 kg were used in the experiment. General anesthesia was induced by venous injection of sodium thiopental associated with subcutaneous injection of ketamine. Blood was collected from cutaneous femoral veins for the preparation of autologous PRP. In each case, 10 μL of PRP and 1 μL of autologous thrombin (SmartPrePTM, Harvest, Plymouth, Mass) were prepared. This was mixed with crushed bone obtained from the chin region of the animals' lower jaws for use as filling around implants. The third left maxillary incisors were removed, and the surrounding alveolar bone was ablated with a round bur to create bone defects measuring 40 × 12 mm. Defects then received titanium implants (TiUnite Mark III, Nobel Biocare, Göthenberg, Sweden) 3.75 mm in diameter and 10 mm in length with a mechanically roughened surface together with autologous filler material. Wounds were then closed by suturing. Calcein (Wako Pure Chemical Industries, Osaka, Japan) at a concentration of 20 mg/kg body weight was administered to the animals by intraperitoneal injection in physiological saline solution 7 days before the collection of specimens. Three days before sacrifice of animals, alizarin red (Wako Pure Chemical Industries) at 40 mg/kg body weight in physiological saline was also administered by intraperitoneal injection. Animals were sacrificed by overdose with sodium pentobarbital 4, 8, and 12 weeks postoperatively.

Preparation of specimens

Maxillary bones containing implants were dissected free of the animals and fixed in 10% phosphate buffered formalin. Bone samples were then trimmed to a convenient size with a micro cutting machine (Exakt 30/784, EXAKT Vertriebs GmbH, Norderstedt, Germany) and were dehydrated with graded ethanol alcohols. Specimens were then embedded in polymethyl methacrylate resin and cut longitudinally along the center of the long axis, again with the micro cutting machine (Exakt). Sample surfaces were ground with 1200-grit silicon carbide paper and polished with 5 almina paste. They were then further polished with discs of sandpaper of progressively smaller grain to prepare 500-μm thick undecalcified sections.

Confocal laser scanning microscopy

Samples were examined by using an inverted CLSM (LSM-GB200, Olympus, Tokyo, Japan) with 6 separate detection strategies but in all cases applying an excitatory argon laser wavelength of 488 nm. In one detection mode (condition 1), both a 535-nm pass filter (CH1) and a 590-nm barrier filter (CH2) were used. Calcein was detected as a greenish color on CH1 and alizarin red appeared as a reddish color on CH2. Detection condition 2 retained the 535-nm pass filter for CH1 but removed the filter for collected

CH2 and then collected images by using both channels together. In detection condition 3, the filter for CH1 was removed, but the 590-nm barrier filter was retained for CH2, and again images for both channels were obtained together. For detection condition 4, both the 535-nm and 590-nm filters were removed, and reflected light only, which was collected through CH2, recorded as a bluish color. Detection condition 5 was a composite achieved by superimposition of the images obtained from both detection conditions 2 and 4. Detection condition 6 was also achieved by superimposition of previously collected images, but in this case the images from detection conditions 1 and 4 were used.

Results

Calcein and alizarin red were readily detected by CLSM in specimens. The animals were treated with calcein and alizarin red 7 and 3 days before sacrifice, respectively. Figure 1 shows newly formed bone was present around a titanium implant at 8 weeks after implantation. Calcein fluorescence is recorded as green fluorescence, whereas alizarin red labeling is seen as red. Where both labels are present in the same location, yellow is seen. The implant surface could not be positively detected by this detection method alone, with the position of the implant inferred only by the dark screwlike profile.

Detection conditions 2 and 3 each revealed calcein and alizarin red staining, respectively, as well as the reflective implant surface. Calcein and alizarin red were also detected independent of one another in detection conditions 2 and 3. The highly reflective implant surface was detected as a prominent red by detection condition 2 (Figure 1B) and as blue by detection condition 3 (Figure 1C).

The detected position of the implant surface was not changed by different detection conditions. Figure 1D shows the reflected image from detection condition 4, in which the only significant signal detected was that reflected from the implant surface. To ensure perfect concordance in detection of the implant with different detection approaches, the reflected image from detection condition 4 (Figure 1D) was superimposed with that gathered in detection condition 2 (Figure 1B) to achieve detection condition 5 (Figure 1E). Significantly, there was perfect concordance creating purple in the composite image (Figure 1E). Also, the green image for calcein was readily seen in relation to the implant (Figure 1E).

Detection condition 6 permitted visualization of both calcein and alizarin red labeling together with the implant. Having confirmed that the position of the implant was identical regardless of the detection method used, superimposition of images from detection conditions 1 and 4 were performed to allow visualization of both calcein and alizarin red labeling together with the precise location of the implant (Figure 1F). The Table summarizes the filter settings and outcomes for each of the detection conditions used.

Bone formed towards the implant 4 weeks after implantation. Figure 2 is typical for the appearance of specimens observed with detection condition 6 at 4 weeks after implantation. There was an annular pattern of bone formation, with the direction of bone formation indicated by sequential calcein and alizarin red labeling as being initially close to the bone and moving towards the implant surface. A wide gap between new bone and the implant was evident, measuring from 200 to 500 μm in width (Figure 2).

Fine processes of new bone were seen contacting the implant by 8 weeks after implantation. At 8 weeks after implantation, fine processes of bone were seen extending through to the implant surface (Figure 1F). Once having reached the implant, these fine processes appeared to extend along the implant surface as extended sheets, with the temporal pattern of growth indicated by the incorporation of calcein and alizarin red (Figures 3A and B). Interestingly, a noncalcified tissue (small gap) of about 10 μm was seen separating this new bone from the implant surface (Figure 3C).

By 12 weeks, bony processes were obscured by new bone growth. The fine bony processes seen 8 weeks after implantation were obscured, and the screw thread areas were filled by new bone formation by the 12th postoperative week (Figure 4A). The newly formed bone was spread from the processes along the implant surface towards the outward direction of lateral existing bone (Figure 4B).

Discussion

The CLSM technique utilized in this study enabled observation of 0.1-μm thick sectional images at intervals of 1 μm any distance from the implant surface. This was accomplished without chemical damage from decalcification, loss of organic matter, or physical damage, which would result if the implants had to be removed from the specimens. In other words, it was possible to observe

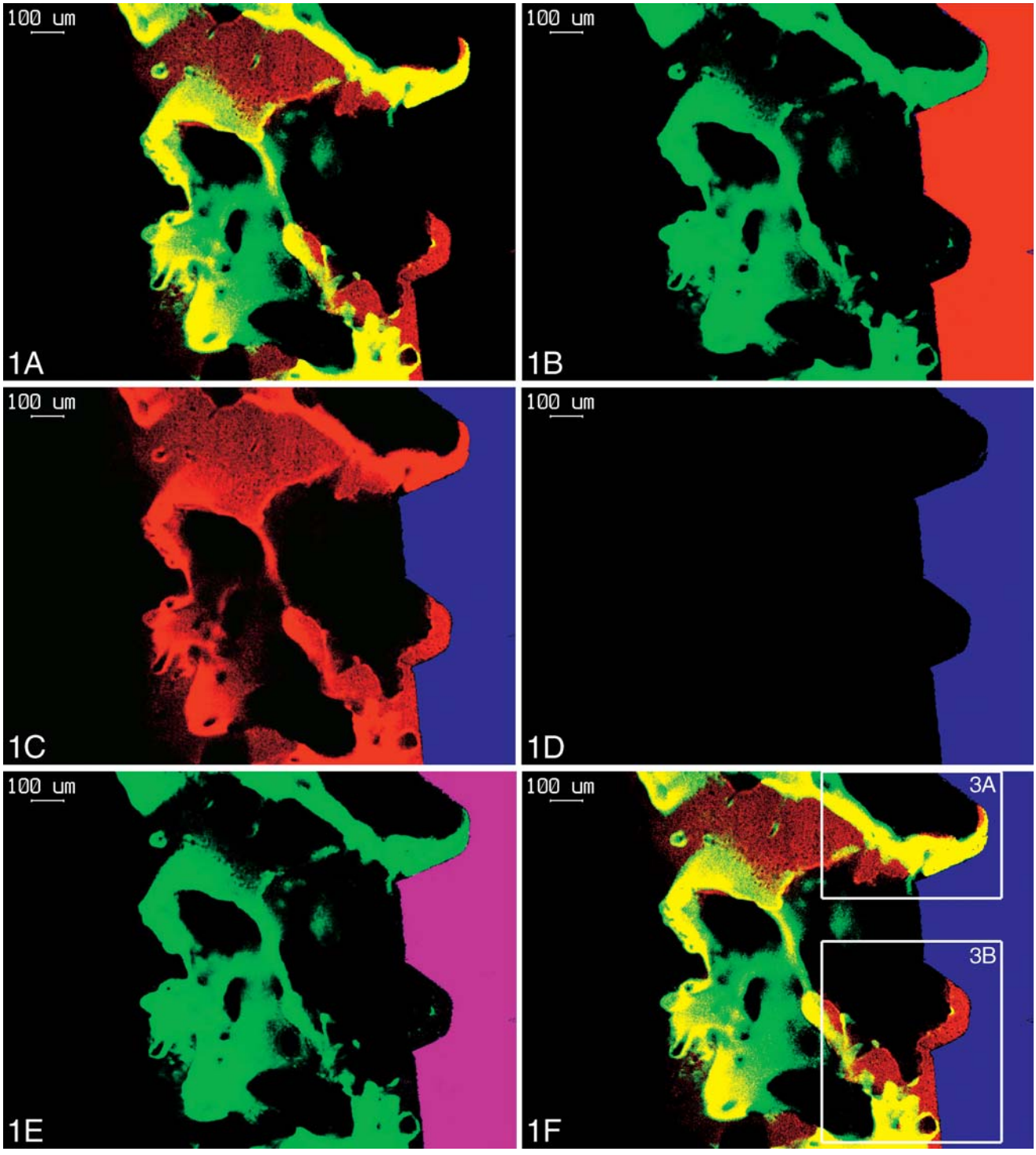

FIGURE 1. Confocal laser scanning microscopy images with detection conditions 1 to 6 (see the Table) of an implant 8 weeks after surgery. (A) Both calcein and alizarin red are detected, but the implant is devoid of the reactions in condition 1. (B and C) Calcein and alizarin red are detected together with the implant in detection conditions 2 and 3, respectively. (D) The highly reflective image is limited to the implant surface in detection condition 4. (E) Superimposition of the reflective implant image of 1B (red) with 1D (blue) is seen as purple in detection condition 5. (F) This image was subsequently used to assess calcein and alizarin red fluorescence, together with reflection of the implant surface, by combining images collected for detection conditions 1 and 4.

TABLE

Filter settings for both channels 1 and 2 for detection conditions 1 to 6, as well as the image components detected being calcein (Ca), alizarin red (AR), or implant (Im)

Detection Condition	Filter Settings			Detected
	CH1	CH2	CH2	
1	535 nm (green)	590 nm (red)		Ca, AR
2	535 nm (green)		Nonfilter (red)	Ca, Im
3		590 nm (red)	Nonfilter (blue)	AR, Im
4			Nonfilter (blue)	Im
5	535 nm (green)		Nonfilter (purple)	Ca, Im
6*	535 nm (green)	590 nm (red)	Nonfilter (blue)	Ca, AR, Im

*By combining images collected with different detection conditions, it was possible to achieve a composite image in condition 6, in which all 3 major elements of the specimen could be detected.

peri-implant calcification in intact bone.[21] By staggering the time of administration of the 2 fluorescent dyes used, the timing and direction of calcification of bone could be observed with reasonable accuracy.

Use of a 488-nm excitation wavelength from an argon laser together with appropriate dyes and filters permitted detection of reflected or fluorescent light of 3 separate wavelengths. Reflected light (488 nm) was seen from the polished metal surface, whereas calcein deposits were detected at 535 nm and alizarin red was seen at 590 nm fluorescence. It is important to note that the intensity of reflected light from the highly polished mirrorlike titanium implant was very high, so that the reflected light was stronger than any fluorescence from the bone. This was exploited to collect data for the position of the implants irrespective of bony fluorescence.

Calcification of bone in an annular pattern as well as in the formation of fine processes was observed, with processes moving towards the implant surface and then spreading across the implants as fine sheets. In annular bone formation during early healing, it is thought that bone forms on the external side of blood vessels in connective tissue, and that the lumen inside these rings become calcified and smaller over time. Thus, it seems that by 8 weeks some of the new bony processes reach the implant surface, with subsequent proliferation along the surface.[22] Sequential staining with calcein followed by alizarin red away from the implant surface indicate an outward direction of later bone formation. This was in agreement with reports suggesting that there is storage of bone directly contacting the implant surface, followed by outward extension from the implant.[7] Thus, bone formation around the implant occurred in 3 directions, initially from the existing bone towards the implant, then extending along the implant surface after reaching the implant, and then finally extending from the implant towards the existing bone. The end effect of this was that by 12 weeks after implantation, new bone was formed that filled the screw-shaped defect.

In the present study, a space of at least 10 μm was found between the implant surfaces and bone. Well-developed connective tissue containing blood vessels and osteoblasts is thought to be interposed between the new bone and implants.[23,24] Very few cells are reported at the interface, but cellular processes from osteocytes are described to approach the titanium oxide,[25] and bone proteins such as osteocalcin and osteopontin are also reported.[26] It is thought that growth factors related to bone formation as well as nutrients required for new bone growth originate from the side of the existing bone, though supply from the implant side cannot be ruled out. Considering that dental implants are constantly exposed to occlusal forces, this space is thought to function as a buffer between the new bone and the implant surface, providing mechanical stimulation and promoting bone formation.[27,28]

In the present study, it was confirmed that new bone extended from existing bone and formed to correspond with the external shape of the implant, and it was also seen that that there was a space of about 10 μm between the new bone and the implant surface. Significantly, this was the first time that the CLSM method simultaneously captured an image of both implant metals and new bone formation.

CONCLUSIONS

The CLSM method enabled observation of the morphology in the process of calcification at the implant surface and surrounding tissues and suggested that there may be significant further applications for this approach.

ACKNOWLEDGMENTS

The authors would like to thank Dr H. Zoellner at Department of Oral Pathology, Faculty of Dentistry, University of Sydney, for his suggestions of this work. A part of this study was financially supported by the Oral Implant Research Grant (Tamaki

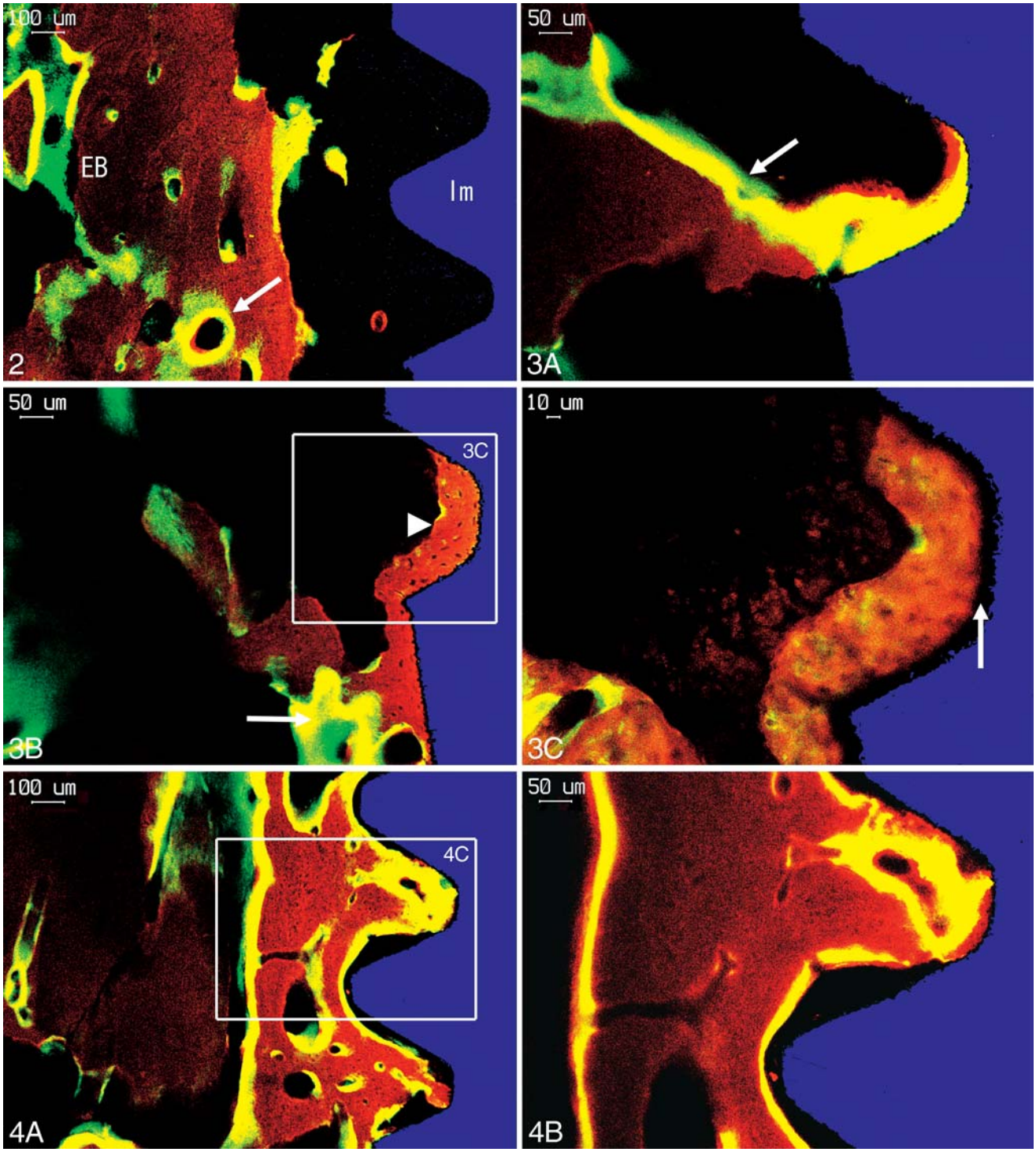

FIGURES 2–4. FIGURE 2. Confocal laser scanning microscopy image observed with detection condition 6 of an implant 4 weeks after surgery. Bone formation is seen to proceed in an annular fashion (arrow) from the existing bone (EB) towards the implant surface (Im). FIGURE 3. Confocal laser scanning microscopy image observed with detection condition 6 of an implant 8 weeks after surgery. Figure 3 pictures are higher magnification of Figure 1F. (A) The process (arrow) extends from existing bone towards the implant surface. (B) Bone proliferation initiates from the new bone (arrow) and progresses across the implant surface (arrowhead). (C) Higher magnification of Figure 3B. The relation between the implant surface and newly formed bone. There is a 10-μm gap separating (arrow) between the implant and bone. FIGURE 4. Confocal laser scanning microscopy image observed with detection condition 6 of an implant 12 weeks after surgery. (A) Bone formation extended throughout the entire region adjacent to the implant surface. (B) Higher magnification of Figure 4A. These areas confirm the annular pattern of bone formation.

Foundation) and Osaka Dental University Joint Research Funds.

References

1. Morris HF, Winkler S, Ochi S, Kanaan A. A new implant designed to maximize contact with trabecular bone: survival to 18 months. *J Oral Implantol.* 2001;27:164–173.

2. Winker S, Ring K, Ring JD, Boberick KG. Implant screw mechanics and the settling effect: an overview. *J Oral Implantol.* 2003;29:242–245.

3. Pretorius JA, Melsen B, Nel JC, Germishuys PJ. A histomorphometric evaluation of factors influencing the healing of bony defects surrounding implants. *Int J Oral Maxillofac Implants.* 2005;20:387–398.

4. Giavaresi G, Ambrosi L, Battiston GA, et al. Histomorphometric, ultrastructural and microhardness evaluation of the osseointegration of a nanostructured titanium oxide coating by metal-organic chemical vapour deposition: an in vivo study. *Biomaterials.* 2004;25:5583–5591.

5. Degidi M, Petrone G, Iezzi G, Piattelli A. Bone contact around acid-etched implants: a histological and histomorphometrical evaluation of two human-retrieved implants. *J Oral Implantol.* 2003;29:13–18.

6. Fini M, Savarino L, Aldini NN, et al. Biomechanical and histomorphometric investigation on two morphologically differing titanium surfaces with and without fluorohydroxyapatite coating: an experimental study in sheep tibiae. *Biomaterials.* 2003;24:3183–3192.

7. Puleo DA, Nanci A. Understanding and controlling the bone-implant interface. *Biomaterials.* 1999;20:2311–2321.

8. Hansson HA, Alberktsson T, Branemark PI. Structural aspects of the interface between tissue and titanium implants. *J Prosthet Dent.* 1983;50:108–113.

9. Albrektsson TO, Johansson CB, Sennerby L. Biological aspects of implant dentistry: osseointegration. *Periodontol 2000.* 1994;4:58–73.

10. Gil-Albarova J, Garrido-Lahiguera R, Salinas AJ, et al. The in vivo performance of a sol-gel glass and a glass-ceramic in the treatment of limited bone defects. *Biomaterials.* 2004;25:4639–4645.

11. Fukuda M, Iino M, Ohnuki T, et al. Vertical alveolar distraction osteogenesis with complications in a reconstructed mandible. *J Oral Implantol.* 2003; 29:185–188.

12. Xiang W, Baolin L, Yan J, Yang X. The effect of bone morphogenetic protein on osseointegration of titanium implants. *J Oral Maxillofac Surg.* 1993;51: 647–651.

13. Listgarten MA, Buser D, Steinemann SG, et al. Light and transmission electron microscopy of the intact interfaces between non-submerged titanium-coated epoxy resin implants and bone or gingiva. *J Dent Res.* 1992;71:364–371.

14. Piattelli M, Scarano A, Paolantonio M, et al. Bone response to machined and resorbable blast material titanium implants: an experimental study in rabbits. *J Oral Implantol.* 2002;28:2–8.

15. Sennerby L, Dasmah A, Larsson B, Iverhed M. Bone tissue responses to surface-modified zirconia implants: a histomorphometric and removal torque study in the rabbit. *Clin Implant Dent Relat Res.* 2005;7:S13–S20.

16. Suzuki K, Aoki K, Ohya K. Effects of surface roughness of titanium implants on bone remodeling activity of femur in rabbits. *Bone.* 1997;21:507–514.

17. Yagishita H, Iwatsubo S, Aoba T. Confocal laser scanning microscopic studies on alveolar bone remodeling with orthodontic tooth movement and retention. *Scanning Microsc.* 1995;9:781–788.

18. Iyama S, Takeshita F, Ayukawa Y, et al. A study of the regional distribution of bone formed around hydroxyapatite implants in the tibiae of streptozotocin-induced diabetic rats using multiple fluorescent labeling and confocal laser scanning microscopy. *J Periodontol.* 1997; 68:1169–1175.

19. Degidi M, Scarano A, Piattelli M, Piattelli A. Histologic evaluation of an immediately loaded titanium implant retrieved from a human after 6 months in function. *J Oral Implantol.* 2004;30: 289–296.

20. Grageda E. Platelet-rich plasma and bone graft materials: a review and standardized research protocol. *Implant Dent.* 2004;13:301–307.

21. Nishikawa T, Masuno K, Tominaga K, et al. Bone repair analysis in a novel biodegradable hydroxyapatite/collagen composite implanted in bone. *Implant Dent.* 2005;14:252–260.

22. Schupbach P, Glauser R, Rocci A, et al. The human bone-oxidized titanium implant interface: a light microscopic, scanning electron microscopic, backscatter scanning electron microscopic, and energy-dispersive X-ray study of clinically retrieved dental implants. *Clin Implant Dent Relat Res.* 2005;7:S36–S43.

23. Braber ETD, Ruijter JED, Jansen JA. The effect of a subcutaneous silicone rubber implant with shallow surface microgrooves on the surrounding tissues in rabbits. *J Biomed Mater Res.* 1997;37: 539–547.

24. Murai K, Takeshita F, Ayukawa Y, et al. Light and electron microscopic studies of bone-titanium interface in the tibiae of young and mature rats. *J Biomed Mater Res.* 1996;30:523–533.

25. Piattelli A, Trisi P, Passi P, et al. Histochemical and confocal laser scanning microscopy study of the bone-titanium interface: an experimental study in rabbits. *Biomaterials.* 1994;15:194–200.

26. Ayukawa Y, Takeshita F, Inoue T, et al. An immunoelectron microscopic localization of noncollagenous bone proteins (osteocalcin and osteopontin) at the bone-titanium interface of rat tibiae. *J Biomed Mater Res.* 1998;41:111–119.

27. Degidi M, Scarano A, Piatteli M, et al. Bone remodeling in immediately loaded and unloaded titanium dental implants: a histologic and histomorphometric study in humans. *J Oral Implantol.* 2005;16:18–24.

28. Meyer U, Joos U, Mythili J, et al. Ultrastructural characterization of the implant/bone interface of immediately loaded dental implants. *Biomaterials.* 2004;25:1959–1967.